



Contents lists available at ScienceDirect

Optik

journal homepage: [www.elsevier.com/locate/ijleo](http://www.elsevier.com/locate/ijleo)

Original research article

## Evaluation of dosimetric properties of Tb-doped MgF<sub>2</sub> transparent ceramics

Tatsuya Matsuo\*, Takumi Kato, Hiromi Kimura, Fumiya Nakamura, Daisuke Nakauchi, Noriaki Kawaguchi, Takayuki Yanagida

Nara Institute of Science and Technology, 8916-5, Takayama-cho, Ikoma-shi, Nara 630-0192, Japan

### ARTICLE INFO

#### Keywords:

Transparent ceramic  
SPS  
MgF<sub>2</sub>  
Scintillator  
Dosimeter  
Tb

### ABSTRACT

We prepared Tb-doped MgF<sub>2</sub> transparent ceramics by the spark plasma sintering method and then measured optical, scintillation and dosimetric properties. We observed sharp peaks due to 4f-4f transition of Tb<sup>3+</sup> ion in all of photoluminescence (PL), scintillation, optically-stimulated luminescence (OSL) and thermally-stimulated luminescence (TSL). Especially, the 1 and 3 % Tb-doped MgF<sub>2</sub> exhibited 120 times laeger TSL intensity as compared to the 0.01 % Tb-doped MgF<sub>2</sub>. In addition, we confirmed the TSL response of the 1 and 3 % Tb-doped samples was very sensitive to irradiation dose and showed a good linearity from 0.01–1000 mGy.

### 1. Introduction

Phosphor materials have been used to take measurements of ionizing radiations. These phosphors are called scintillators or dosimeters in response to the luminescence phenomena involved. Scintillator is a device that absorbs and converts incident radiation energy to low energy photons immediately. Therefore, radiations can be indirectly measured using scintillator together with a conventional photodetectors such as photomultiplier tube (PMT) or photodiode (PD). We have usually used scintillators in various application fields such as border security [1], medicine [2] and oil-dwelling [3]. On the other hand, phosphor-based dosimeters show storage luminescence phenomena after ionizing radiation exposure. This phenomenon includes thermally-stimulated luminescence (TSL) [4], optically-stimulated luminescence (OSL) [5] and radio-photoluminescence (RPL) [6]. In TSL and OSL, electrons and holes created by interactions with ionizing radiations are trapped at localized trapping centers and stored stably. These carriers are de-trapped by an external stimulation and recombine at emission centers. Phosphor-based dosimeters are mainly put to practical use as personal dosimetry. RPL has the same process of carrier trapping with OSL and TSL but it can show photoluminescence (PL) after the trapping. For that reason, it is important that an effective atomic number ( $Z_{\text{eff}}$ ) of the phosphor is close to that of human soft tissue ( $Z_{\text{eff}} = 7.29$ ) [7]. Although there have been the ideal material with the same  $Z_{\text{eff}}$  of human soft tissue, light materials which possess a close  $Z_{\text{eff}}$  to human body have been utilized for personal dose monitoring.

Magnesium fluoride (MgF<sub>2</sub>) can be applied as a phosphor for personal dosimeters because it has relatively low  $Z_{\text{eff}}$  ( $= 10.46$ ) close to that of human soft tissue [8]. Dosimetric properties of magnesium fluorides (MgF<sub>2</sub>) doped with rare earth and transition metal elements have been studied [9–17]. Among these investigations, we have reported that Eu-doped MgF<sub>2</sub> transparent ceramics had good dosimetric properties [12]. Hence, MgF<sub>2</sub> transparent ceramics doped with Tb<sup>3+</sup> ion which is one of the rare earth elements are also considered to possess good dosimetric properties as is the case of Eu-doped MgF<sub>2</sub>. Because several Tb-doped dosimetric materials such as Mg<sub>2</sub>SiO<sub>4</sub> are known to show high TSL intensity [18], we can expect a high dosimetric performance when we activate Tb<sup>3+</sup> ion

\* Corresponding author.

E-mail address: [matsuo.tatsuya.mn6@ms.naist.jp](mailto:matsuo.tatsuya.mn6@ms.naist.jp) (T. Matsuo).

as a dopant to  $\text{MgF}_2$ .

The aim of this research is to synthesize Tb-doped  $\text{MgF}_2$  transparent ceramics by the spark plasma sintering (SPS) method and investigate the optical, scintillation and dosimetric properties. The SPS method is a relatively new sintering process that is characterized by a rapid consolidation rate, and it has been used to fabricate transparent ceramics [19–22]. In addition, SPS is generally performed in a highly reductive atmosphere, so it can increase the defect concentration which can be expected to work as a trapping center for storage luminescence.

## 2. Experimental

A series of Tb-doped  $\text{MgF}_2$  transparent ceramic samples with different Tb concentrations (0.01, 0.1, 1, 3 and 5 mol.%) were synthesized by the SPS method. A mortar and pestle were used to mix  $\text{MgF}_2$  (4 N) and  $\text{TbF}_3$  (4 N) raw powders. The mixture was loaded in a cylindrical graphite die with a hole with a diameter of 10.4 mm and held between two graphite punches inserted. Then, we sintered the mixture by applying uniaxial pressure and supplying pulse current across the graphite assembly in an SPS furnace (LabX-100, Sinter Land). The temperature was elevated from the room temperature to 550 °C at a heating rate of 100 °C/min under 5.5 MPa pressure and then kept for 10 min. Next, the temperature was further elevated to 750 °C at a heating rate of 100 °C/min under 5.5 MPa pressure and then kept for 7 min. During the synthesis, the sintering temperature was monitored using a K-type thermocouple attached on the graphite die. Wide surfaces of the obtained ceramic samples were polished using a polishing machine (MetaServ 250, BUEHLER), and they were characterized by the following procedures.

A scanning electron microscope (SEM; JEOL JCM-6000plus) was used to observe backscattered electron images. In order to investigate optical properties, transmission spectra were measured by a UV–vis near-infrared spectrophotometer V670 (JASCO Corporation). Quantaaurus-QY (C11347, Hamamatsu Photonics) was used to evaluate photoluminescence (PL) emission and excitation map as well as quantum yields (QYs) under excitations of 250 and 350 nm. PL spectra were measured by a Spectrofluorometer FP8600 (JASCO Corporation) which had a higher wavelength resolution than Quantaaurus-QY. Quantaaurus-Tau (Hamamatsu Photonics) was used to measure PL decay profiles monitoring at 550 nm during 250 nm excitations.

Scintillation spectra were measured by a CCD spectrometer DU-420-BU2 (Andor) and high sensitivity spectrometer Shamrock 163 (Andor) [23]. As the excitation source, an X-ray generator equipped with a W anode target (XRB80P&N200 × 4550, Spellman) and a Be window was used, and the X-ray generator was operated with a tube voltage of 40 kV and current of 1.2 mA. X-ray excited fluorescence lifetime photometer (Hamamatsu Photonics) was used to measure scintillation decay curves [24].

As dosimetric properties, TSL glow curves were measured by a TSL reader (TL-2000, Nanogray Inc.) over the temperature range of 50–490 °C with a heating rate of 1 °C/s [25]. Prior to the measurement, the sample was irradiated by X-rays with a certain dose ranging from 0.01 mGy to 1000 mGy. TSL spectra were measured by a combination of CCD spectrometer QEPro (Ocean Optics) and ceramic heater system (SCR-SHQ-A, Sakaguchi) [26]. OSL spectra were measured by a Spectrofluorometer FP8600 (JASCO Corporation). During the irradiation, we used X-ray ionization chamber (TN30013, PTW) to determine the dose.

## 3. Results and discussion

### 3.1. Sample

Fig. 1(a) shows a photograph of Tb-doped  $\text{MgF}_2$  transparent ceramic samples synthesized in this research. The 0.01 % Tb-doped sample was visibly clear while the highly  $\text{Tb}^{3+}$  doping samples were opaque. In addition, green fluorescence was confirmed under excitation light of 253 nm as indicated in Fig. 1(b). The thickness and the densities of the 0.01, 0.1, 1, 3 and 5 % Tb-doped samples are summarized in Table 1. The difference of thicknesses arose from the fact that the polishing was done individually for each sample by our hands. The densities of the 0.01 and 0.1 % Tb-doped samples were close to a theoretical density of  $\text{MgF}_2$ , and when Tb concentration increases, the density also increased since  $\text{Tb}^{3+}$  ions were heavier than  $\text{Mg}^{2+}$ . A SEM image observed on a fracture

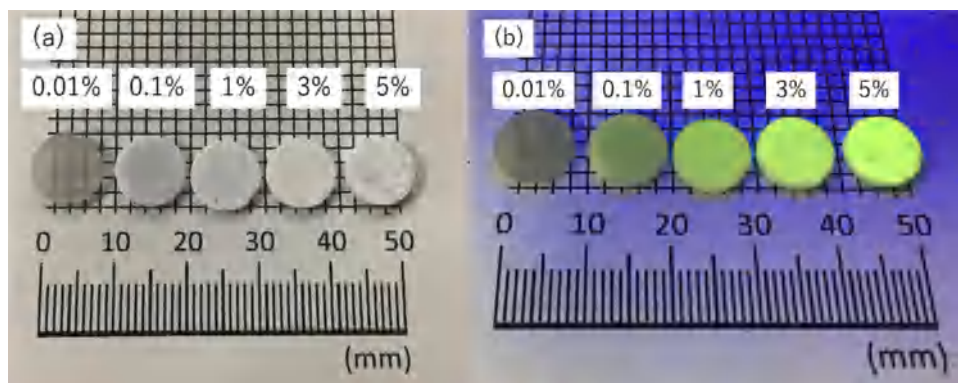


Fig. 1. Synthesized  $\text{MgF}_2$  ceramics doped with  $\text{Tb}^{3+}$  ion (0.01, 0.1, 1, 3 and 5 %) under (a) room light and (b) excitation light of 253 nm.

**Table 1**  
Thickness and densities of Tb-doped MgF<sub>2</sub> ceramic samples.

Sample	Thickness	Density
0.01 % Tb	1.16 mm	3.15 g/cm <sup>3</sup>
0.1 % Tb	1.20 mm	3.15 g/cm <sup>3</sup>
1 % Tb	1.15 mm	3.19 g/cm <sup>3</sup>
3 % Tb	1.19 mm	3.39 g/cm <sup>3</sup>
5 % Tb	1.19 mm	3.39 g/cm <sup>3</sup>

surface of the 5 % Tb-doped MgF<sub>2</sub> ceramic sample is shown in Fig. 2. The SEM image suggests that grain sizes is 1 μm or less. Compared with the grain size of the non-doped MgF<sub>2</sub> ceramic produced by the same manner [10], that of the 5 % Tb-doped MgF<sub>2</sub> ceramic sample was almost the same size.

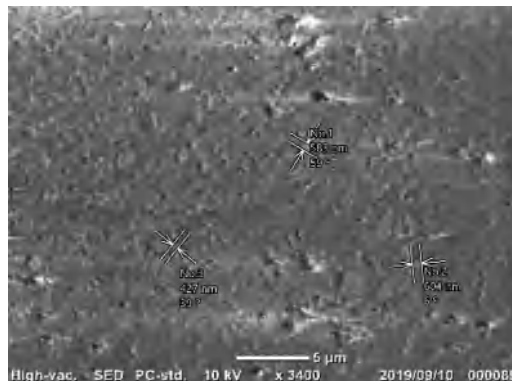
### 3.2. Optical properties

Fig. 3 represents in-line transmittance spectra of Tb-doped MgF<sub>2</sub> transparent ceramic samples. The 0.01 % Tb-doped sample showed a transmittance at least 80 % or more in the near infrared region and also had a transmittance of a several percent in the UV–vis region. On the other hand, the transmittance in the UV–vis region of the samples having the concentration of 0.1 % or more was close to 0 %.

Fig. 4 indicates a PL emission and excitation map of 1 % Tb-doped MgF<sub>2</sub> ceramic sample as an example. An intense emission band around 550 nm appeared under excitation in the range of 250–380 nm. Compared with a previous study, this peak positions coincide with 4f-4f transition of Tb<sup>3+</sup> ion, so it was confirmed that this emission was due to 4f-4f transition of Tb<sup>3+</sup> ion [27]. In addition, we also confirmed that there was no unexpected emission due to impurities and defects. Although intensities were different, spectral features of the othe samples were the same. Fig. 5 shows PL spectra of all Tb-doped MgF<sub>2</sub> ceramic samples. When the monitoring wavelength was 550 nm, the excitation peaks were observed in the range of 200–380 nm including a broad peak at 230 nm and plural sharp peaks from 260 to 380 nm. With reference to the previous study, it was confirmed that the excitation bands in 230 nm were due to 4f-5d transition of Tb<sup>3+</sup> ion, and the peaks in the range of 260–380 were due to 4f-4f transition of Tb<sup>3+</sup> ion [27]. The QYs at 250 and 350 nm excitations are summarized in Table 2. The QY of the 3 % Tb-doped sample was maximum at 350 nm excitation, and the value was 29.6 %. Among the present samples, the highest QY was achieved by Tb 3 % doped sample. Fig. 6 shows PL decay time profiles of Tb-doped MgF<sub>2</sub> ceramic samples. The resulting decay curves were approximated by a single exponential decay function. All the decay time constants were several millisecond, and they were typical decay time due to the 4f-4f transition of the Tb<sup>3+</sup> ion [28].

### 3.3. Scintillation properties

Fig. 7 shows X-ray induced scintillation spectra of Tb-doped MgF<sub>2</sub> ceramic sample. In all the samples, scintillation emission peaks were detected in the range of 450–650 nm as with PL, which were due to the 4f-4f transition of Tb<sup>3+</sup> ions. We could not observe a broad emission peaks due to the self-trapped exciton and defect centers which were observed in the undoped MgF<sub>2</sub> under X-rays irradiation. The emission intensity was proportional to Tb concentration since the stopping power against X-rays simple depended on Z<sub>eff</sub> and the density as well as the scintillation light yield. Fig. 8 demonstrates scintillation decay time profiles of Tb-doped MgF<sub>2</sub> ceramic samples. The obtained decay curves were approximated by a single exponential decay function. All the decay time constants were several millisecond. Although these values were typical as the decay time constant due to the 4f-4f transition of Tb<sup>3+</sup> ion [29], they were shorter than those of PL. However, in general, scintillation decay time is longer than that of PL since the scintillation



**Fig. 2.** SEM image of 5 % Tb-doped MgF<sub>2</sub> ceramic sample.

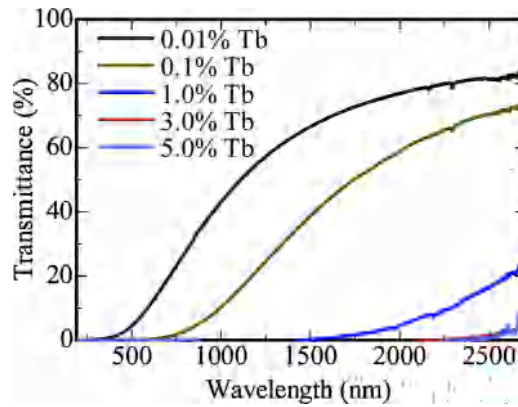


Fig. 3. In-line transmittance spectra of Tb-doped MgF<sub>2</sub> ceramic samples.

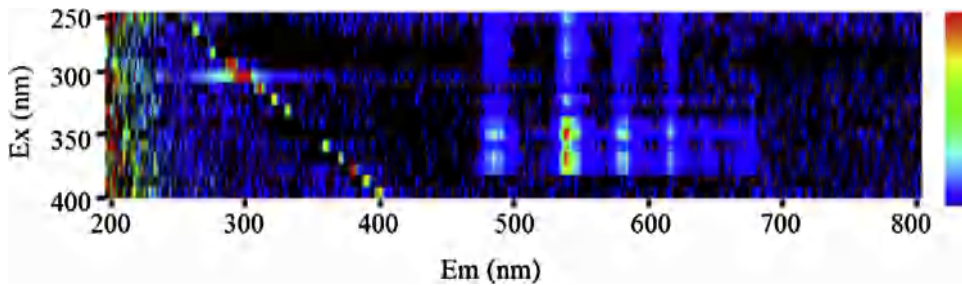


Fig. 4. PL emission (horizontal axis) and excitation (vertical axis) map of 1 % Tb-doped MgF<sub>2</sub> ceramic sample.

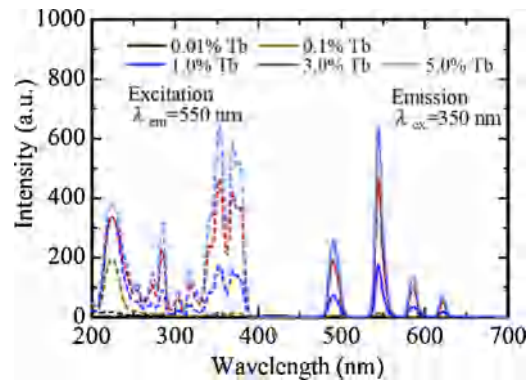


Fig. 5. PL emission and excitation spectra of Tb-doped MgF<sub>2</sub> ceramic samples.

**Table 2**  
QY of Tb-doped MgF<sub>2</sub> ceramic samples.

Sample	QY (Ex.250 nm)	QY (Ex. 350 nm)
0.01 % Tb	2.0 %	0.0 %
0.1 % Tb	3.7 %	1.7 %
1 % Tb	5.6 %	13.1 %
3 % Tb	4.6 %	29.6 %
5 % Tb	4.5 %	25.0 %

process involves energy migration processes while PL does not [30]. In previous papers, this unusual phenomenon could be explained as below [31]. A typical interpretation is that some competitions between the energy transfer and quenching of excited carriers by the interaction among them may occur in the Tb-doped MgF<sub>2</sub> ceramic samples. In the PL, one ultraviolet or visible wavelength photon excited only electrons of the 4f orbital of Tb<sup>3+</sup> ion, and the interaction of excited electrons each other is neglected. Whereas in the scintillation, X-ray generate many secondary electrons (or carriers) in a typical interspatial distance of 10–100 nm, so the interaction

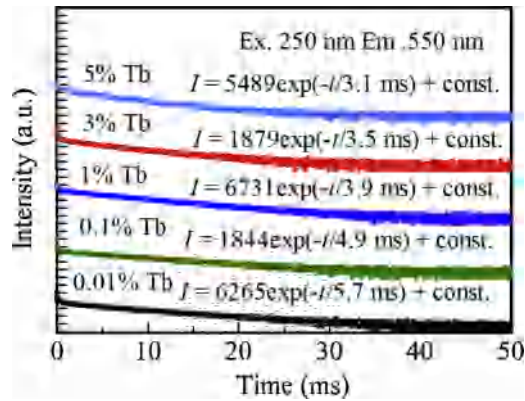


Fig. 6. PL decay time profiles of Tb-doped MgF<sub>2</sub> ceramic samples.

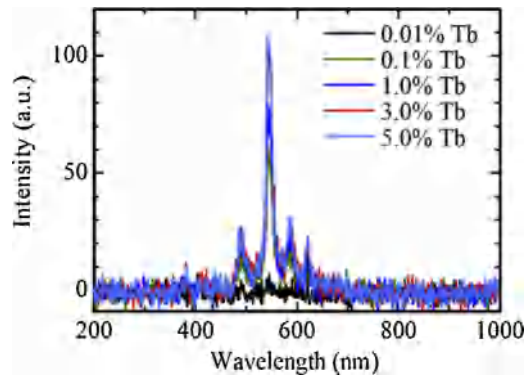


Fig. 7. X-ray induced scintillation spectra of Tb-doped MgF<sub>2</sub> ceramic samples.

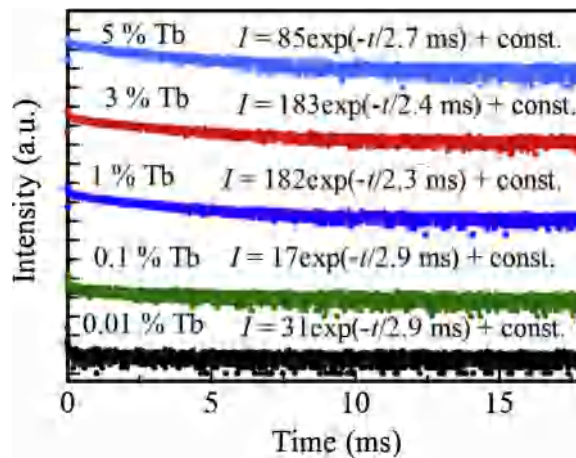


Fig. 8. Scintillation decay time profiles of Tb-doped MgF<sub>2</sub> ceramic samples under pulsed X-ray excitation.

of these excited electrons could not be neglected. In these materials, the quenching processes due to the interaction of the excited secondary electrons would be ascendant.

### 3.4. dosimetric properties

Fig. 9 represents OSL spectra of Tb-doped MgF<sub>2</sub> ceramic samples when the irradiation dose was 1000 mGy. Although an OSL signal could not be confirmed in the 0.01 and 0.1 % Tb-doped samples, the 1.0, 3.0 and 5.0 % Tb-doped samples showed OSL at a stimulation of 620 nm. The emission origin is considered to be the emission due to the 4f-4f transition of Tb<sup>3+</sup> ion. At stimulation wavelength longer than 620 nm, OSL peak due to the 4f-4f transition of Tb<sup>3+</sup> ion was not detected in all the samples.

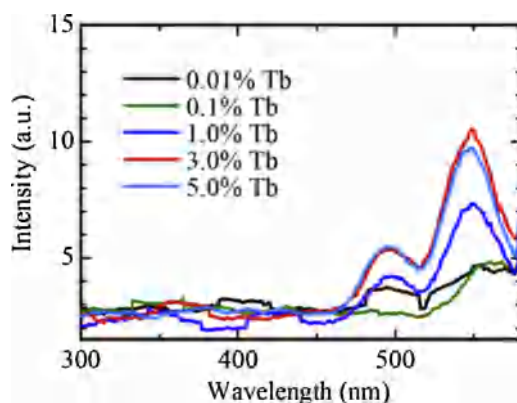


Fig. 9. OSL spectra of Tb-doped MgF<sub>2</sub> ceramic sample when irradiation dose was 1000 mGy.

Fig. 10(a) and (b) shows TSL glow curves of all Tb-doped MgF<sub>2</sub> ceramic samples and TSL glow curve with fitting of 1 % Tb-doped MgF<sub>2</sub> ceramic sample as a representative of all the samples, respectively. Fitting parameter for TSL glow curve of 1 % Tb-doped MgF<sub>2</sub> ceramic sample are shown in Table 3. As a result of fitting analysis using the GCD function [32], glow peaks were detected around 80, 125, 150, 230 and 350 °C for all the samples, although there was a large difference in the intensity of each peak depending on the doping concentration. The glow peaks around 80, 125, 150 and 350 °C were also observed in non-doped MgF<sub>2</sub> transparent ceramic [10], and the origin of these peaks was ascribed to MgF<sub>2</sub> itself. As the glow peak located at 230 °C, the TSL intensity increased as the Tb concentration increased until 3 %, and the TSL intensity of the 1 and 3 % Tb-doped samples was approximately 120 times larger than that of the 0.01 % Tb-doped sample. With reference to a previous study, the glow peak around 230 °C would be due to some kinds of defects generated by doping of Tb<sup>3+</sup> ion. The existence of Tb<sup>3+</sup> ions may distort the lattice with the creation of defects acting as trapping centers, and there is also the creation of charge compensating defects. Moreover, it has been reported that the accumulation rate of F center induced by  $\gamma$ -ray irradiation for Tb-doped MgF<sub>2</sub> crystals is higher than that for non-doped MgF<sub>2</sub> crystals, and the doping Tb<sup>3+</sup> ion into MgF<sub>2</sub> enhances the creation of defects by ionizing radiations [16,33]. When we compare with Eu-doped MgF<sub>2</sub> transparent ceramic [8], the glow peak temperature of Tb-doped one is preferable and is comparable to commercial TSL dosimeters [34].

Fig. 11 demonstrates TSL spectra of Tb-doped MgF<sub>2</sub> ceramic sample heated at 230 °C. As in the PL and scintillation spectra, sharp emission peaks in the range of 450–650 nm were confirmed in TSL. This result suggests that the emission center is Tb<sup>3+</sup> ion also in the TSL process. TSL dose response curves of Tb-doped MgF<sub>2</sub> ceramic samples are shown in Fig. 12. The irradiated dose range was from 0.01–1000 mGy. Good linearity in the range of 1–1000 mGy for 0.01 % Tb-doped sample, in the range of 0.1–1000 mGy for 0.1 and 5 % Tb-doped samples and in the range of 0.01–1000 mGy for 1 and 3 % Tb-doped ones were confirmed. In comparison with the sensitivity of Eu-doped MgF<sub>2</sub> transparent ceramic, the 1 and 3 % Tb-doped samples have the same sensitivity (lower detection limit of 0.01 mGy) [12]. Here, it should be noted that this is a higher sensitivity with commercial personal dosimeters since the detection limit of typical commercial dosimeters for personnel dose monitoring applications is 0.1 mGy [35].

#### 4. Conclusions

Tb-doped MgF<sub>2</sub> transparent ceramics with different Tb concentrations (0.01, 0.1, 1, 3 and 5 mol.%) were prepared by the SPS method, and optical, scintillation and dosimetric properties were investigated. In both PL and scintillation properties, emission peaks arose from the 4f-4f transition of Tb<sup>3+</sup> ion were observed in the range of 450–600 nm, having the decay time constant of a few

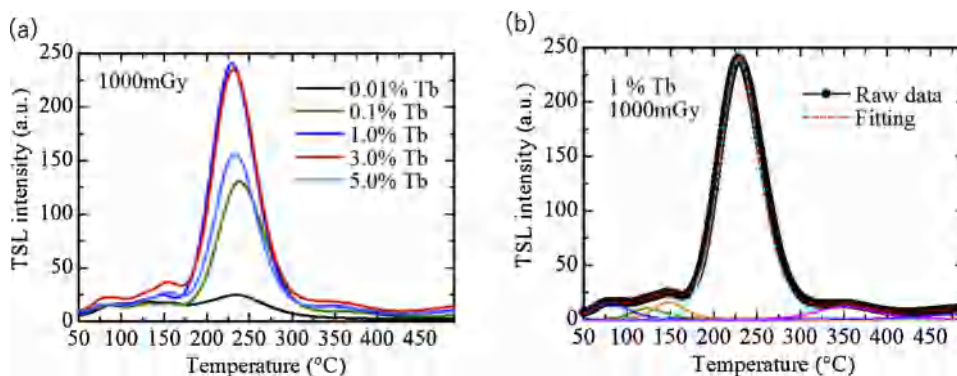
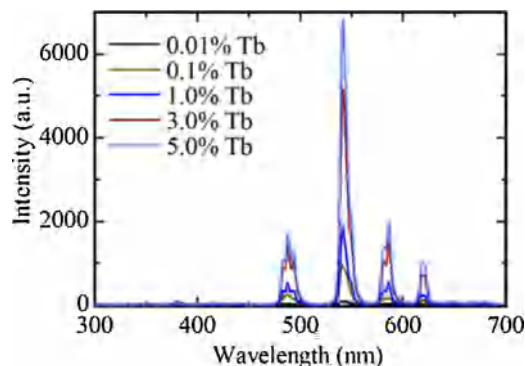
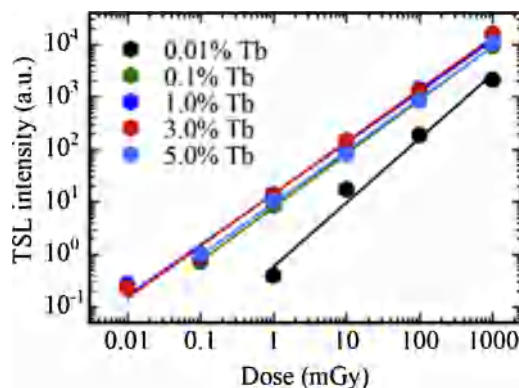


Fig. 10. (a). TSL glow curves of Tb-doped MgF<sub>2</sub> ceramic samples and (b). 1 % Tb-doped MgF<sub>2</sub> ceramic samples with fitting functions.

**Table 3**Fitting parameter for TSL glow curve of 1 % Tb-doped MgF<sub>2</sub> ceramic sample.

	Peak1	Peak2	Peak3	Peak4	Peak5	Peak6
$T_m$ (°C)	80	124	148	229	352	485
$I_m$ (a.u.)	14.7	10.3	16	240	12	4.7
$E$ (eV)	0.7	1	1.18	1.3	1.35	1.4

**Fig. 11.** TSL spectra of Tb-doped MgF<sub>2</sub> ceramic samples heated at 230 °C.**Fig. 12.** TSL dose response curves of Tb-doped MgF<sub>2</sub> ceramic samples.

milli-second. As dosimetric properties, the Tb-doped MgF<sub>2</sub> ceramic samples showed OSL having the emission peaks around 550 nm due to the 4f-4f transitions of Tb<sup>3+</sup> ion at the stimulation of 620 nm. Furthermore, the Tb-doped MgF<sub>2</sub> ceramic samples had excellent TSL properties. TSL spectra clearly showed that the emission origin in TSL process was 4f-4f transition of Tb<sup>3+</sup>. Moreover, it was demonstrated that the optimum Tb-doping concentration was from approximately 1–3% judging from the comparison of TSL intensities and dose responses.

### Declaration of Competing Interest

The authors declare that they have no known competing financial interests or personal relationships that could have appeared to influence the work reported in this paper.

### Acknowledgements

This work was supported by Grant-in-Aid for Scientific Research A (17H01375), Scientific Research B (18H03468 and 19H03533) and JSPS Fellows (19J22091) from JSPS. The Cooperative Research Project of Cooperative Research Project of Research Center for Biomedical Engineering, Murata Foundation, Iketani Foundation, Nippon Sheet Glass Foundation and NAIST foundation are also acknowledged.

## References

- [1] D. Totsuka, T. Yanagida, K. Fukuda, N. Kawaguchi, Y. Fujimoto, J. Pejchal, Y. Yokota, A. Yoshikawa, Performance test of Si PIN photodiode line scanner for thermal neutron detection, *Nucl. Instruments Methods Phys. Res. Sect. A Accel. Spectrometers, Detect. Assoc. Equip.* 659 (2011) 399–402, <https://doi.org/10.1016/j.nima.2011.08.014>.
- [2] T. Yanagida, A. Yoshikawa, Y. Yokota, K. Kamada, Y. Usuki, S. Yamamoto, M. Miyake, M. Baba, K. Kumagai, K. Sasaki, M. Ito, N. Abe, Y. Fujimoto, S. Maeo, Y. Furuya, H. Tanaka, A. Fukabori, T. Rodrigues dos Santos, M. Takeda, N. Ohuchi, Development of Pr:LuAG scintillator array and assembly for positron emission mammography, *IEEE trans. Nucl. Sci.* 57 (2010) 1492–1495, <https://doi.org/10.1109/TNS.2009.2032265>.
- [3] C.L. Melcher, Scintillators for well logging applications, *Nucl. Instruments Methods Phys. Res. Sect. B Beam Interact. with Mater. Atoms.* 40–41 (1989) 1214–1218, [https://doi.org/10.1016/0168-583X\(89\)90622-8](https://doi.org/10.1016/0168-583X(89)90622-8).
- [4] S.W.S. McKeever, *Thermoluminescence of Solids*, Cambridge Univ. Press, 1988.
- [5] H. von Seggern, Photostimulable x-ray storage phosphors: a review of present understanding, *Brazilian J. Phys.* 29 (1999) 254–268, <https://doi.org/10.1590/s0103-97331999000200008>.
- [6] G. Belev, G. Okada, D. Tonchev, C. Koughia, C. Varoy, A. Edgar, T. Wysokinski, D. Chapman, S. Kasap, Valency conversion of samarium ions under high dose synchrotron generated X-ray radiation, *Phys. Status Solidi Curr. Top. Solid State Phys.* 8 (2011) 2822–2825, <https://doi.org/10.1002/pssc.201084103>.
- [7] C.A. Jayachandran, Calculated effective atomic number and Kerma values for tissue-equivalent and dosimetry materials, *Phys. Med. Biol.* 16 (1971) 617–623, <https://doi.org/10.1088/0031-9155/16/4/005>.
- [8] M. Kurudirek, Effective atomic numbers and electron densities of some human tissues and dosimetric materials for mean energies of various radiation sources relevant to radiotherapy and medical applications, *Radiat. Phys. Chem.* 102 (2014) 139–146, <https://doi.org/10.1016/j.radphyschem.2014.04.033>.
- [9] M. Secu, S. Jipa, C.E. Secu, T. Zaharescu, R. Georgescu, M. Cutrubinis, Processes involved in the high-temperature thermoluminescence of a Mn<sup>2+</sup>-doped MgF<sub>2</sub> phosphor, *Phys. Status Solidi Basic Res.* 245 (2008) 159–162, <https://doi.org/10.1002/pssb.200743108>.
- [10] F. Nakamura, T. Kato, G. Okada, N. Kawaguchi, K. Fukuda, T. Yanagida, Scintillation, TSL and RPL properties of MgF<sub>2</sub> transparent ceramic and single crystal, *Ceram. Int.* 43 (2017) 7211–7215, <https://doi.org/10.1016/j.ceramint.2017.03.009>.
- [11] G. Okada, F. Nakamura, N. Kawano, N. Kawaguchi, S. Kasap, T. Yanagida, Radiation-induced luminescence centres in Sm:MgF<sub>2</sub> ceramics, *Nucl. Instruments Methods Phys. Res. Sect. B Beam Interact. with Mater. Atoms.* 435 (2018) 268–272, <https://doi.org/10.1016/j.nimb.2018.01.032>.
- [12] F. Nakamura, T. Kato, G. Okada, N. Kawaguchi, K. Fukuda, T. Yanagida, Scintillation and TSL properties of MgF<sub>2</sub> transparent ceramics doped with Eu<sup>2+</sup> synthesized by spark plasma sintering, *J. Alloys. Compd.* 726 (2017) 67–73, <https://doi.org/10.1016/j.jallcom.2017.07.320>.
- [13] F. Nakamura, T. Kato, G. Okada, N. Kawano, N. Kawaguchi, K. Fukuda, T. Yanagida, Scintillation, dosimeter and optical properties of MgF<sub>2</sub> transparent ceramics doped with Gd<sup>3+</sup>, *Mater. Res. Bull.* 98 (2018) 83–88, <https://doi.org/10.1016/j.materresbull.2017.09.058>.
- [14] F. Nakamura, T. Kato, G. Okada, N. Kawaguchi, K. Fukuda, T. Yanagida, Scintillation and storage luminescence properties of MgF<sub>2</sub> transparent ceramics doped with Ce<sup>3+</sup>, *Opt. Mater. (Amst)* 72 (2017) 470–475, <https://doi.org/10.1016/j.optmat.2017.06.043>.
- [15] W. Chen, S.L. Westcott, S. Wang, Y. Liu, Dose dependent x-ray luminescence in MgF<sub>2</sub>: Eu<sup>2+</sup>, Mn<sup>2+</sup> phosphors, *J. Appl. Phys.* 103 (2008), <https://doi.org/10.1063/1.2937084>.
- [16] L.G. Jacobsohn, A.L. Roy, C.L. McPherson, C.J. Kucera, L.C. Oliveira, E.G. Yukihara, J. Ballato, Rare earth-doped nanocrystalline MgF<sub>2</sub>: synthesis, luminescence and thermoluminescence, *Opt. Mater. (Amst)* 35 (2013) 2461–2464, <https://doi.org/10.1016/j.optmat.2013.06.045>.
- [17] M. Secu, C.E. Secu, S. Jipa, T. Zaharescu, M. Cutrubinis, High temperature thermoluminescence of Mn<sup>2+</sup>-doped MgF<sub>2</sub> for personal dosimetry, *Radiat. Meas.* 43 (2008) 383–386, <https://doi.org/10.1016/j.radmeas.2007.11.047>.
- [18] S. Akca, Z.G. Portakal, T. Dogan, N. Kucuk, A. Canimoglu, M. Topaksu, N. Can, Thermoluminescence properties of Tb doped Mg<sub>2</sub>SiO<sub>4</sub> after beta irradiation, *Nucl. Instruments Methods Phys. Res. Sect. B Beam Interact. with Mater. Atoms.* 458 (2019) 12–20, <https://doi.org/10.1016/j.nimb.2019.07.042>.
- [19] D. Jiang, D.M. Hulbert, U. Anselmi-Tamburini, T. Ng, D. Land, A.K. Mukherjee, Optically transparent polycrystalline Al<sub>2</sub>O<sub>3</sub> produced by spark plasma sintering, *J. Am. Ceram. Soc.* 91 (2008) 151–154, <https://doi.org/10.1111/j.1551-2916.2007.02086.x>.
- [20] Y. Futami, T. Yanagida, Y. Fujimoto, J. Pejchal, M. Sugiyama, S. Kurosawa, Y. Yokota, A. Ito, A. Yoshikawa, T. Goto, Optical and scintillation properties of Sc<sub>2</sub>O<sub>3</sub>, Y<sub>2</sub>O<sub>3</sub> and Lu<sub>2</sub>O<sub>3</sub> transparent ceramics synthesized by SPS method, *Radiat. Meas.* 55 (2013) 136–140, <https://doi.org/10.1016/j.radmeas.2013.01.014>.
- [21] G. Toci, M. Vannini, M. Ciofini, A. Lapucci, A. Pirri, A. Ito, T. Goto, A. Yoshikawa, A. Ikesue, G. Alombert-Goget, Y. Guyot, G. Boulon, Nd<sup>3+</sup>-doped Lu<sub>2</sub>O<sub>3</sub> transparent sesquioxide ceramics elaborated by the Spark Plasma Sintering (SPS) method, *Opt. Mater. (Amst)* 41 (2015) 12–16, <https://doi.org/10.1016/j.optmat.2014.09.033>.
- [22] S. Grasso, H. Yoshida, H. Porwal, Y. Sakka, M. Reece, Highly transparent  $\alpha$ -alumina obtained by low cost high pressure SPS, *Ceram. Int.* 39 (2013) 3243–3248, <https://doi.org/10.1016/j.ceramint.2012.10.012>.
- [23] T. Yanagida, K. Kamada, Y. Fujimoto, H. Yagi, T. Yanagitani, Comparative study of ceramic and single crystal Ce:GAGG scintillator, *Opt. Mater. (Amst)* 35 (2013) 2480–2485, <https://doi.org/10.1016/j.optmat.2013.07.002>.
- [24] T. Yanagida, Y. Fujimoto, T. Ito, K. Uchiyama, K. Mori, Development of X-ray-induced afterglow characterization system, *Appl. Phys. Express.* 7 (2014) 62401, <https://doi.org/10.7567/APEX.7.062401>.
- [25] T. Yanagida, Y. Fujimoto, N. Kawaguchi, S. Yanagida, Dosimeter properties of AlN, *J. Ceram. Soc. Japan.* 121 (2013) 988–991, <https://doi.org/10.2109/jcersj2.121.988>.
- [26] G. Okada, T. Kato, D. Nakauchi, K. Fukuda, T. Yanagida, Photochromism and thermally and optically stimulated luminescences of AlN ceramic plate for UV sensing, *Sensors Mater.* 28 (2016) 897–904, <https://doi.org/10.18494/SAM.2016.1250>.
- [27] G. Okada, K. Shinozaki, T. Komatsu, N. Kawano, N. Kawaguchi, T. Yanagida, Tb<sup>3+</sup>-doped BaF<sub>2</sub>-Al<sub>2</sub>O<sub>3</sub>-B<sub>2</sub>O<sub>3</sub> glass and glass-ceramic for radiation measurements, *J. Non. Solids* 501 (2018) 111–115, <https://doi.org/10.1016/j.jnoncrysol.2018.02.013>.
- [28] M. Back, M. Boffelli, A. Massari, R. Marin, F. Enrichi, P. Riello, Energy transfer between Tb<sup>3+</sup> and Eu<sup>3+</sup> in co-doped Y<sub>2</sub>O<sub>3</sub> nanocrystals prepared by Pechini method, *J. Nanopart. Res.* 15 (2013), <https://doi.org/10.1007/s11051-013-1753-8>.
- [29] N. Kawano, T. Kato, G. Okada, N. Kawaguchi, T. Yanagida, Optical, scintillation and dosimeter properties of MgO:Tb translucent ceramics synthesized by the SPS method, *Opt. Mater. (Amst)* 73 (2017) 364–370, <https://doi.org/10.1016/j.optmat.2017.08.025>.
- [30] M. Koshimizu, K. Iwamatsu, M. Taguchi, S. Kurashima, A. Kimura, T. Yanagida, Y. Fujimoto, K. Watanabe, K. Asai, Influence of linear energy transfer on the scintillation decay behavior in a lithium glass scintillator, *J. Lumin.* 169 (2016) 678–681, <https://doi.org/10.1016/j.jlumin.2015.04.015>.
- [31] N. Kumamoto, D. Nakauchi, T. Kato, G. Okada, N. Kawaguchi, T. Yanagida, Photoluminescence, scintillation and thermally-stimulated luminescence properties of Tb-doped 12CaO·7Al<sub>2</sub>O<sub>3</sub> single crystals grown by FZ method, *J. Rare Earths.* 35 (2017) 957–963, [https://doi.org/10.1016/S1002-0721\(17\)60999-2](https://doi.org/10.1016/S1002-0721(17)60999-2).
- [32] G. Kitis, J.M. Gomez-Ros, J.W.N. Tuyn, Thermoluminescence glow-curve deconvolution functions for first, second and general orders of kinetics, *J. Phys. D Appl. Phys.* 31 (1998) 2636–2641, <https://doi.org/10.1088/0022-3727/31/19/037>.
- [33] I. Nuritdinov, M.A. Mussaeva, V.M. Reiterov, Radiation-induced accumulation of structural defects in MgF<sub>2</sub> crystals doped with rare-earth impurities, *Opt. Spectrosc.* 86 (1999) 219 (2019) 1–2.
- [34] T. Yanagida, G. Okada, N. Kawaguchi, Ionizing-radiation-induced storage-luminescence for dosimetric applications, *J. Lumin.* 207 (2019) 14–21, <https://doi.org/10.1016/j.jlumin.2018.11.004>.
- [35] From the homepage of Chiyoda Technol Corp. [http://www.c-technol.co.jp/cms/wp-content/uploads/2019/09/glass\\_2019](http://www.c-technol.co.jp/cms/wp-content/uploads/2019/09/glass_2019) (n.d.).